Korean J. Chem. Eng., 40(5), 1086-1093 (2023)
DOI: 10.1007/s11814-022-1254-5

pISSN: 0256-1115
eISSN: 1975-7220

Bioinspired spindle-knotted structure fiber membrane prepared by modified coaxial electrospinning for water-in-oil emulsion separation

Sufeng Wei*,‡, Zhengzheng Xu,‡, Yan Liu***, Yunhong Liang***, and Guoyong Wang**,†**

*Key Laboratory of Advanced Structural Materials, Changchun University of Technology, Changchun, 130012, P. R. China
**Key Laboratory of Automobile Materials, Department of Materials Science and Engineering, Jilin University, Changchun, 130025, P. R. China
***Key Laboratory of Bionic Engineering (Ministry of Education) and State Key Laboratory of Automotive Simulation and Control, Jilin University, Changchun 130022, P. R. China
(*Received 24 May 2022 • Revised 6 August 2022 • Accepted 10 August 2022*)

Abstract−Inspired by the conformation of spider silks, fibers with multiscale spindle-knotted structures were fabricated via a one-step modified coaxial electrospinning method. Under a high-voltage electric field, hydrophobic silica polystyrene (PS) fibers coated poly (methyl methacrylate) (PMMA) fibers were integrated together during the electrospinning process. Due to the addition of hydrophobic gaseous SiO_2 combining the spindle structure, a superhydrophobic fibrous membrane was prepared, and the bioinspired fibers achieved a superhydrophobic/superoleophilic performance for efficient emulsion separation. The results demonstrate that the incorporation of PS and SiO_2 improved the efficiency of emulsion separation of the fabricated fibrous membranes by optimizing microstructure and wettability: Specifically, an extraordinary water contact angle under oil (162°) and a satisfied oil contact angle under water (0°). For water-in-diesel emulsions, a high separation efficiency of 99.1% was obtained for membrane with PS addition of 4 wt%, which is greater than of pure PVDF membrane with SiO_2 (75.5%). It performs better than most other membranes showing strong promise in grease purification and oily wastewater treatment.

Keywords: Coaxial Electricity, Bionic, Superhydrophobic, Superoleophilic

INTRODUCTION

With the increase in industrial oily wastewater and the frequent occurrence of oil spill accidents, oily wastewater has become a worldwide problem [1,2]. More efforts have been made to separate the oil/water mixture and emulsion. Traditional oil/water separation technologies mainly use air flotation, oil skimming combined with gravity separation, oil absorbing materials, etc. [3,4]. However, due to poor separation efficiency, high energy consumption, and complex separation apparatus, these methods are not efficient for oil-water emulsion separation [5-7]. Emulsified oil/water mixtures are commonly inactive and stable oil-in-water or water-in-oil emulsions with droplet sizes ranging from nanometers to microns. Therefore, the separation of oil-water emulsions has been difficult. In particular, water-in-oil emulsions with large number of dispersed water droplets and particle size less than 20 μm in the oil phase are very stable and difficult to separate successfully, which remains a worldwide challenge [8].

In recent years, membrane materials with special wettability have received considerable attention in oil/water and emulsion separation and are considered to be one of the most promising approaches to resolve the above problems [9,10]. Membranes with high hydrophobicity have good oil affinity and water repellency to remove water from immiscible oil-water mixtures [11-13]. Although many membrane materials with superhydrophobicity have been successfully prepared, they can only separate the oil layer from the oil-water mixture because of their large pore size. For surfactant-stabilized water-in-oil emulsions, most of them are inadequate. Besides the superhydrophobic properties of the membrane, a suitable porosity is a key factor of achieving effective emulsion separation [14,15].

Naseed et al. prepared porous PAN-GO-SiO_2 membranes and proposed that the addition of SiO_2 can improve the roughness of the fibers [16]. Fang et al. prepared HBPU/F/SiO_2 membranes that a switchable wettability membrane was obtained by electrospinning. The addition of fluorinated SiO_2 here improves the roughness on one hand, and increases the contact angle of the membranes on the other [17]. Although the increase in roughness is critical to improve the wettability state of the surface at the macroscopic level, it has almost no effect on tiny water droplets at microscopic scale. This is because when the droplet dimension is too small, the droplet state on the surface will more probably alternate from Cassie state to Wenzel, accordingly diminishing the superhydrophobic properties [18,19]. The droplets are then more likely to be pinned to the surface and not be able to move smoothly [20]. Zhang et al. reported a COF-Dha Tab/PAN composite spindle-knotted membrane for the effective separation of water-in-oil and oil-in-water emulsions [21]. Recently, Zhang et al. organized TiO_2-PVPA.nNa spindle nanocomposite used to separate the water from water-in-oil emulsion.

†To whom correspondence should be addressed.
E-mail: materwanggy@jlu.edu.cn
‡These authors contributed equally to this work and should be considered co-first authors.

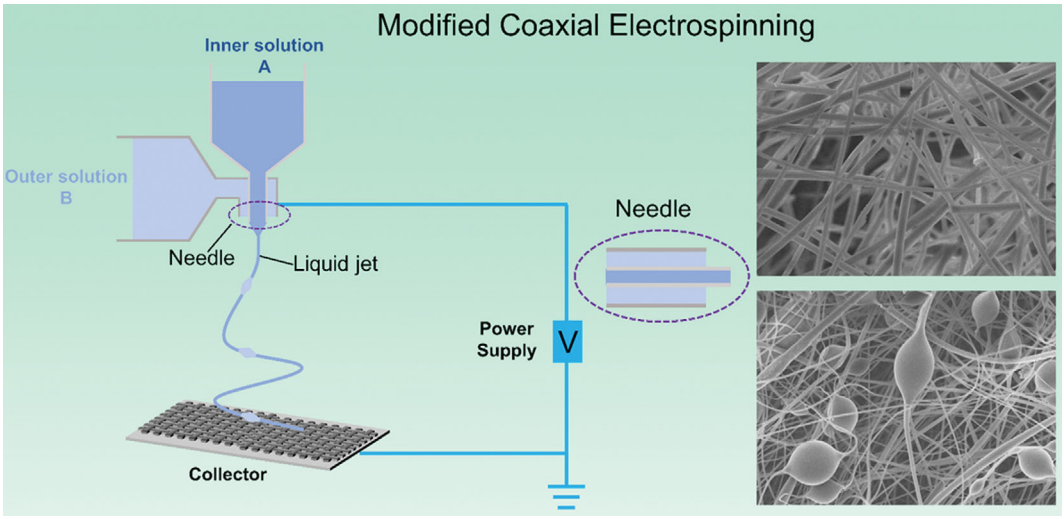

Scheme 1. Preparation of the spindle-knotted fibrous membranes with coaxial electrospinning.

This separation is achieved by tiny water collecting and leaving on the superhydrophobic spindle structure [22]. The separation efficiency is as executed as 95.68% due to the appropriate pore size and the presence of spindle knotted structures. However, due to the low porosity of this membrane, the separation of the emulsion can only be carried out with extra pressure. How to prepare a superhydrophobic spindle structured membrane in an inexpensive way is a problem that enables the effective separation of emulsions without extra force. There are few reviews on this in the current study.

Herein, considering the facile fabrication and extensive application of poly (methyl methacrylate) (PMMA) and polystyrene (PS), we prepared superhydrophobic spindle structured membranes by homemade protruding coaxial needles blended with hydrophobic SiO_2. In this study, we used steady PMMA once as the inner solution, with low cost PS and hydrophobic SiO_2 as the outer solution (Scheme 1), and prepared a superhydrophobic membrane with steady spindle structured membranes by this coaxial electrospinning method. This membrane has a water contact angle of 162° and an oil contact angle of nearly 0°. The developed membrane can achieve efficient separation of emulsions underneath the motion of gravity. This is rarely mentioned in the current literature. Superhydrophobic PMMA/PS/SiO_2 membranes with spindle-knotted structures were expected to provide an effective strategy to separate steady nano-emulsions and industrial oily wastewater in practice.

EXPERIMENT SECTION

1. Materials

All chemicals and solvents were purchased from commercial suppliers without further purification. Deionized water made by us was used for all experiments, poly (methyl methacrylate) (PMMA) and polystyrene (PS) were purchased from Aladdin Industrial Corporation, hydrophobic SiO_2 particles (product code: A200; average primary particle size: 12 nm) were supplied by Degussa. N, N-dimethylformamide (DMF, ≥99.5%,) purchased from China Pharmaceutical (Group) Shanghai Chemical Reagent Company Co., Ltd. (China), span-80 purchased from Sinopec Nanjing Chemical Industry Co. Ltd. (China), tetrahydrofuran (THF), anhydrous ethanol, acetone and methanol were Beijing Tongguang Fine Chemical Company (China).

2. Preparation of Bioinspired Spindle-knotted Structured Fibrous Membranes

Preparation of PMMA in the inner solution A: Mixed DMF and THF in a 4 : 1 ratio, and used the mixture as the solvent. The inner solution A was prepared by mixing 400 mg of PMMA in 10 g solvent (4 wt%) under continuous stirring at 800 r/min for 2 h at 25 °C.

Preparation of PS/SiO_2 in the outer solution B: Mixed DMF and THF in a 4 : 1 ratio, and used the mixture as the solvent. Added 400 mg (4 wt%) hydrophobic SiO_2 in 10 g solvent of outer solution B as the precursor solution. Then mixed 0, 200, 600, 800 mg of PS (0, 2, 6, 8 wt%) in the above 10 g precursor solution B, respectively, under continuous stirring at 800 r/min for 2 h at 25 °C. The amounts of materials in spinning solution A and solution B are listed in Table 1. Samples with different concentration as described in the Table 1 were defined as S1-S4.

Fabrication of PMMA/PS/SiO_2 fibrous membranes: A homemade coaxial electrospinning apparatus, as illustrated in Scheme 1, was used in this study. The as-prepared electrospinning solution B was loaded into the outer plastic syringe, while the inner plastic syringe was loaded with solution A. The coaxial needle consists of a 27# stainless steel needle as the inner needle and a 20# stainless steel needle as the outer needle, and the tip of the inner needle protrudes outward by 0.5 mm [23]. Using a flat stainless steel mesh as a fiber collector, we placed about 20 cm from the tip of the coaxial needle. The feed rate of solution A was precisely controlled with a syringe pumped at a constant velocity of 3 ml/h, while the feed rate of solution B was 2 ml/h, too. A DC voltage of 15 Kv was applied between the needle and the collector at room temperature, about 25 °C, resulting in stable and continuous PMMA/PS/SiO_2 fibrous membranes.

3. Water-in-oil Emulsion Separation Experiments

Water-in-oil emulsion was prepared for the following procedure. First, 1 ml water (2 wt%) was dissolved in 50 ml diesel, then 0.1 ml Span 80 (0.2 wt%) was added into the oil. After stirring vio-

Table 1. Composition of spinning solution

Sample	Inner solution A	Outer solution B		Solvent	
	PMMA (g)	PS (g)	SiO_2 (g)	DMF (g)	THF (g)
S1	0.400	0.400	0.000	8.000	2.000
S2	0.400	0.400	0.200	8.000	2.000
S3	0.400	0.400	0.600	8.000	2.000
S4	0.400	0.400	0.800	8.000	2.000

lently for 4 h, stable surfactant-stabilized water-in-oil emulsion was obtained successfully. All surfactant-stabilized water-in-oil emulsions were stable for more than three months without demulsification observed. For separation, each prepared membrane was sealed between two vertical glass tubes with inner diameter of 20 mm and sealed with a silicon liner. The newly prepared 10 ml emulsion was poured on the membrane to make it automatically and rapidly permeated by gravity. The oil could pass through the membrane to be harvested in the receiving vessel, while the water droplets were blocked above the membrane. Finally, the water-in-oil emulsion was successfully separated. The separation efficiency of as prepared superhydrophobic fibrous membranes for the water-in-oil emulsion was calculated by the formula [24]:

$$f = \frac{C_0 - C_1}{C_0} \times 100\% \quad (1)$$

where C_0 and C_1 are the water concentration of the original water-in-oil emulsion and the collected water concentration after separation, respectively.

4. Characterization Techniques

The membrane was prepared via electrospinning machine SS-2535H (Beijing Yongkang Leye Technology Development Co., Ltd, China), the surface morphology of the samples was observed by a field emission scanning electron microscope (FE-SEM, JEOL JSM-6700F). During the FE-SEM measurement, the operating voltage and distance was 8 Kv and 8 mm, respectively. The average surface roughness (Ra) was characterized by LEXT OLS300 (Olympus Corporation), the optical images were captured by a digital camera (Nikon D5500). Static contact angle and sliding angle were collected with 5 μl drops of water (JC 2000A Powereach, China). Residual water size images before and after water-in-oil emulsion separation were obtained by Zeiss microscope.

RESULTS AND DISCUSSION

1. Construction of Superhydrophobic Membrane with Spindle-knotted Structures

The morphology and structure of the spindle with different PS

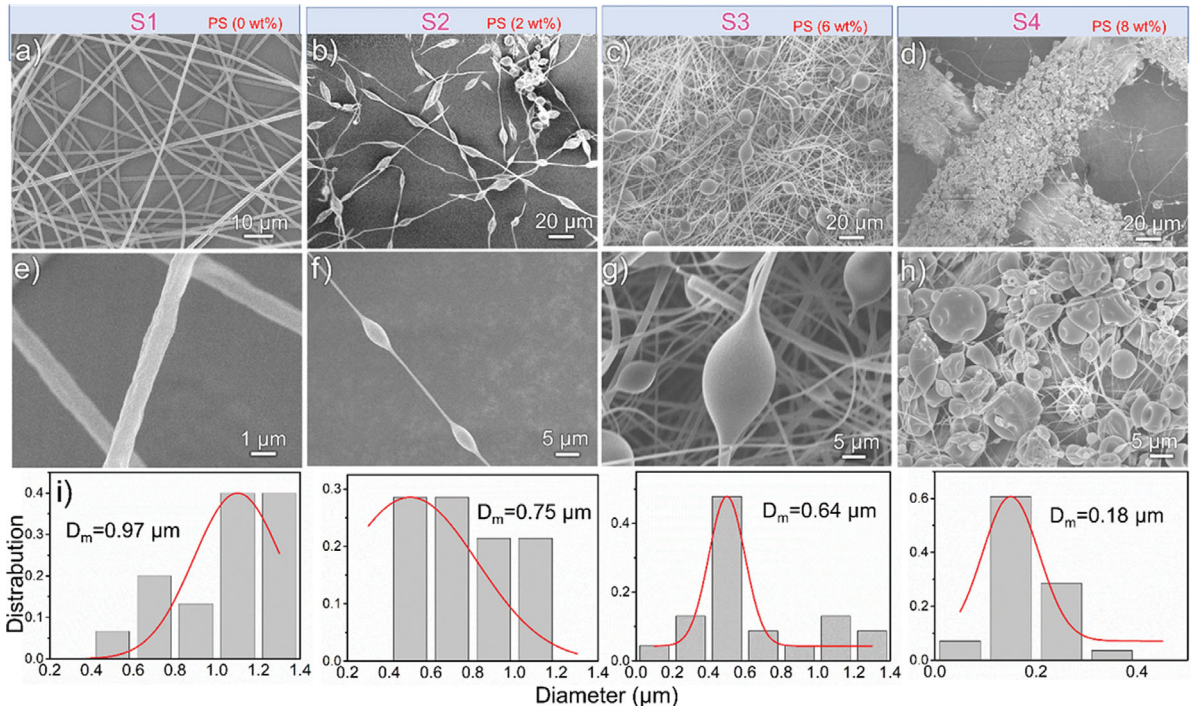

Fig. 1. FE-SEM images of surface with different concentration of PS. (a) and (e) are images of surface S1 without PS. (b) and (f) are images of surface S2 with PS of 2 wt%. (c) and (g) are images of surface S3 with PS of 6 wt%, (d) and (h) are images of surfaces S4 with PS of 8 wt%. (i) is the size distribution of the fiber diameter corresponding with (a) to (d).

concentrations were investigated, as shown in Fig. 1. First, a uniform PS/PMMA nanofibrous membrane was fabricated from coaxial electrospinning method of the inner solution A combined outer solution B, which only contained SiO_2 just as Fig. 1(a) and Fig. 1(e) show, which was named S1. Subsequently, extra optimized dilute PS solutions with different content (2, 6, 8 wt%) were prepared in the above outer solution B to construct the spindle-knots fiber membrane. With the increase of PS concentration, the size of the spindle-knots was increased while the size of the fiber diameter decreased. During the electrospinning process, the mean diameter (D_m) and surface morphology of the fibers can be controlled by adjusting the PS concentration in the solution. It can be clearly observed that the average diameter of the fibers gradually decreased from 0.97 μm to 0.13 μm (Fig. 1(j)) with increasing the high-viscosity of PS concentration from 2% to 8%. Thus, the higher PS concentration of the outer solution B can result in narrower fiber diameters due to the high-viscosity of PS. High-resolution FE-SEM micrographs of the individual PS spindle-knots are shown in the insets. The higher the PS concentration of the outer solution B, the larger were the spindle-knots (Fig. 1(f) to Fig. 1(h)). It can be seen from Fig. 1 that the width of the spindle-knots is inversely proportional to the width of the fiber. The surfaces are all smooth from the enlarged image (Fig. 1(e) to Fig. 1(h)). When the PS concentration was 2 wt% (S2), the spindle-knots size was uniform, the ratio of the spindle-knots and the fibers were spindly; when the PS concentration was 6 wt% (S3), the spindle-knots were more rounded, the ratios of the spindle-knots and the fibers were more different as shown in Fig. 1(c) and Fig. 1(g); when the PS concentration increased to 8 wt% (S4), the spindle-knots were very unstable, and the fibers were slim. In the process of coaxial electrostatic spinning, the viscosity of the outer solution increased in the PS concentration, and the spindle-knots increased and widened, while the fibers were slimmed under control of force. From Fig. 1, the S3 membranes were formed by adding 6 wt% PS and had a better shape and uniform filament size, so this concentration was chosen to prepare the fiber membrane with spindle-knots.

Because the inner needle of coaxial electrostatic spinning protrudes more than the outer one, corner flow is formed into the protruding part of the inner needle [25,26]. This flow manifests in the form of liquid threads with the smoothly varying curvature spreading along the side fences and then distributing over other available corners. Upon invading the diverging channel along the inner needle, the outer solution fills it up rather fast. However, as the outer solution continues to flow along the inner needle, it can be arrested by the corner. As the fluid is replenished, the pressure increases and the pinned outer solution accumulates on the corner. The outer solution bulges up near the arrested edge, thus creating more surface area and, consequently, more surface free energy. This bulging up leads to a hydraulic jump that results in an increase of the local contact angle. The pinned edge moves forward when the local contact angle is greater than a critical value determined by the intrinsic contact angle and the slope of the pinned edge. And when the pinned edge is successfully free of pinning, the outer solution flows down and combines with the inner solution. Depending on the viscosity and surface energy of the outer solution, it bulges with different degrees as they accumulate and forms different shapes of the surface of the inner solution as Fig. 2(a) shows. Fig. 2(b) shows a typical spindle structure FE-SEM images formed by the modified coaxial electrospinning.

Different PS concentration on the outer solution leads to different solution viscosity, resulting in the accumulation of different amounts to solution at the corner flow position. Different spindle-knotted

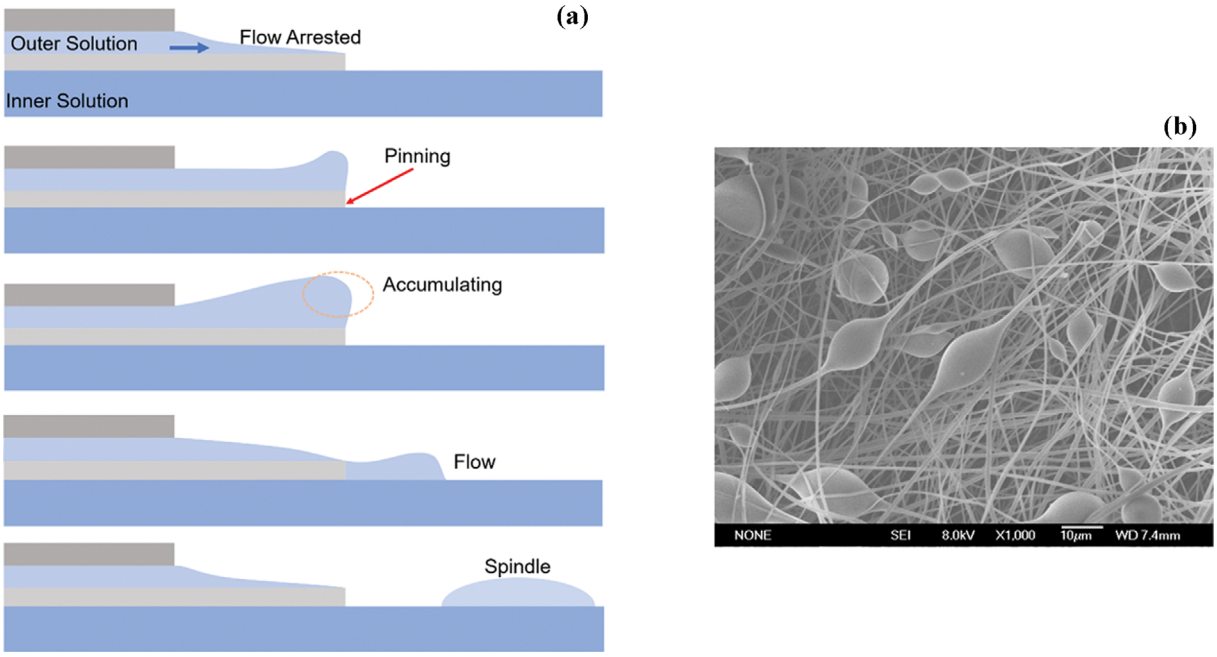

Fig. 2. (a) Schematic drawing showing the spreading of a primary droplet in the forward direction, which consists of pinning of the advancing edge, accumulating, flowing and cutting off to form spindle structure. (b) The FE-SEM image of a typical spindle structure made by the coaxial electrostatic spinning.

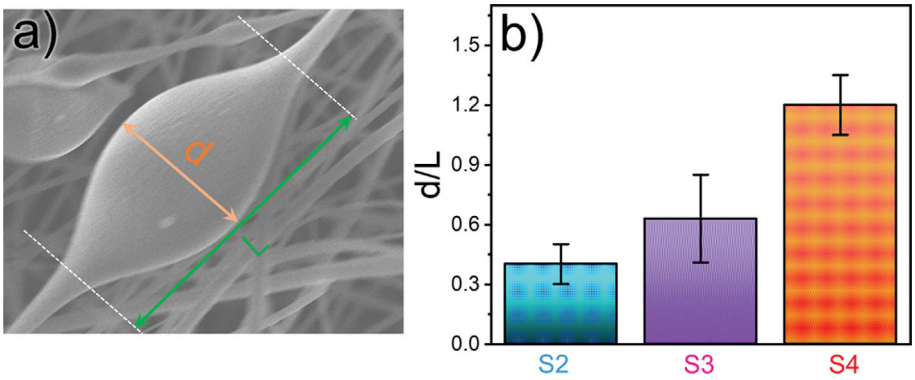

Fig. 3. (a) Naming the length (L) and diameter (d) of the spindle. (b) The ratio of lengths of diameters of different spindles (S2, S3, S4).

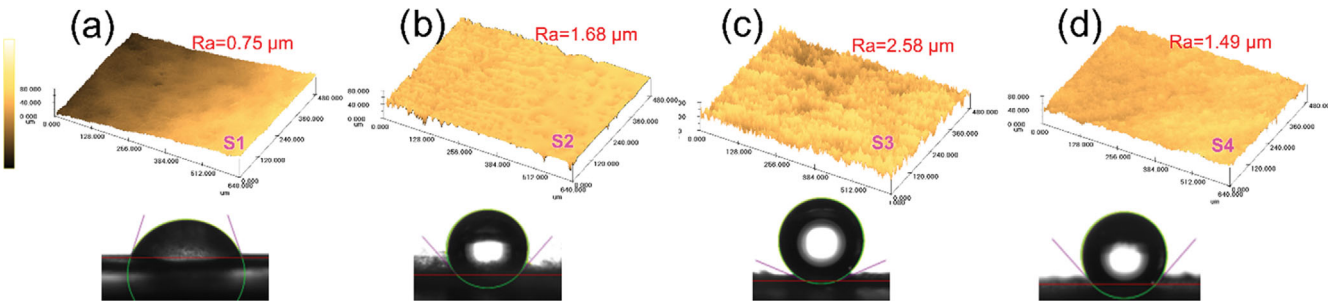

Fig. 4. (a) CLSM images and WCA of the membranes: (a) S1, (b) S2, (c) S3 and (d) S4.

structures were obtained according to different outer solution concentrations, and the ratio of the diameter (d) to the length (L) was defined as d/L as shown in Fig. 3(a). To explore an optimized condition, different weight ratios of PS and solvent from 0.2 to 0.8 were prepared. On S2 membranes, the d/L is 0.40±0.11. The spindle was elongated now (Fig. 1(b)). Further increasing the PS content leads to a slight increase in d/L, which goes up to 0.63±0.22 on S3 membranes. The spindle was rounded now (Fig. 1(c)). When the ratio increased to 0.8 (S4), the d/L increased to 1.22±0.15. The spindle was almost aspherical (Fig. 1(d)). This should be due to the concentration of the outer solution, resulting in too much viscosity. It can be seen that the d/L increases to the concentration of the PS in the outer solution, as shown in Fig. 3(b).

2. The Wettability Properties of Spindle-knotted Structured Membranes

Fig. 4 shows surface roughness and water contact angle (WAC) of the membranes. With the increase of the PS in the outer solution, the Ra values of the membranes increased from 0.75 μm to 2.58 μm and then decreased to 1.49 μm, as shown in the upper right corner of each illustration of Fig. 4. As a result, the more PS wrapped in outer solution was attributed to the spindle increased, the fiber diameter decreased, then the surface roughness first increased and then decreased. The pure PMMA fibrous membranes had the lowest WCA (72±3°), as shown in Fig. 4(a), corresponding to the lowest surface roughness. As the addition of PS increased in outer solution, WCA of membranes increased, and the 6 wt% PS fiber membranes had the highest WCA, as shown in Fig. 4(c). The results indicate that adding PS in the outer solution increased the hydrophobicity of the spindle membranes in coaxial electrospinning and the S3 membrane had the best hydrophobicity of all the samples prepared.

Fig. 5 shows the wettability of S3 membrane to water and oil in the air and in water environment, respectively. The wettability of water on S3 membrane in the air environment is presented in Fig. 5(a), which shows that an oil droplet spread over the surface, while the water droplet dyed blue was spherical on it. It can be seen that an oil droplet is quickly absorbed by the S3 membrane in water environment (Fig. 5(b)). And water droplet remained spherical on S3 surface when the membrane was in the oil environment as shown in Fig. 5(c). These wettability images confirm that S3 membrane has a high adsorption to oil droplets, and it also has high repellency to water droplets in air, water and oil environments, which confirms its suitability for water-in-oil filtration applications. In the air, when water droplets contact S3 membrane, the water droplets are spherical and will not be adsorbed by S3 membrane even if pressed more, and can successfully escape from the surface of S3 after unloading, indicating that S3 membrane has a good ability to repel water in the air as shown in Fig. 5(d). Similarly, in the air, when an oil droplet contacts the S3 membrane, the oil droplet is immediately adsorbed, and it is permeated by the S3 membrane as shown in Fig. 5(e). Under the oil (diesel), a water droplet adhesion experiment was also done, and when the water droplet contacted the S3 membrane surface, it still appeared spherical. Water droplet could be easily detached after unloading after loading as shown in Fig. 5(f). In the water, the oil droplet spread out rapidly on S3 membrane and it penetrated rapidly in 1 second, as shown in Fig. 5(g). These results provide a basic condition for the separation of water-in-oil emulsion.

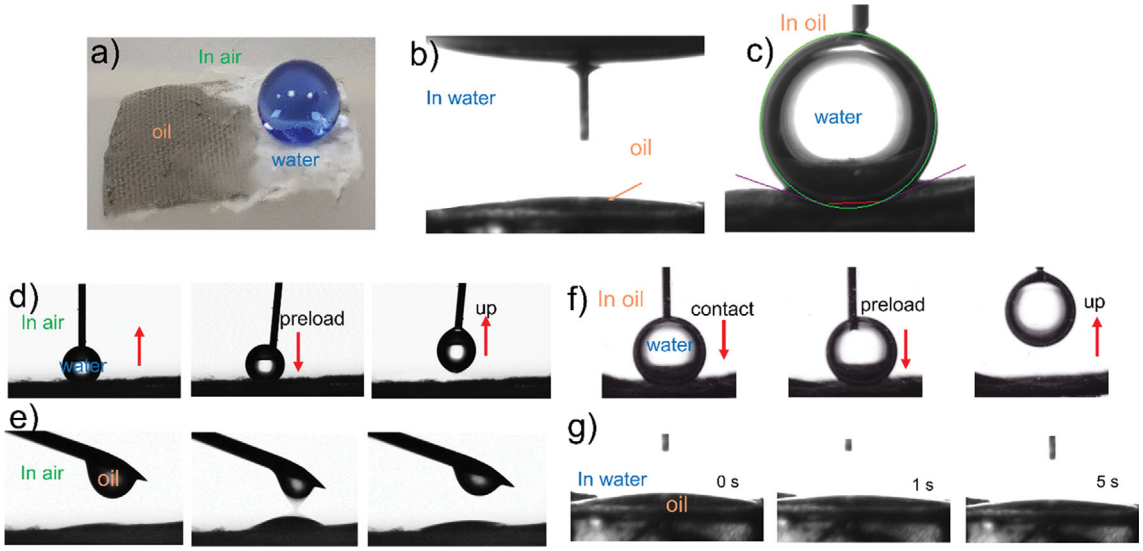

Fig. 5. (a) The oil and water contact angle of spindle-knotted structure membrane in the air; (b) The oil contact angle in the water; (c) The water contact angle in the oil on F2 membranes. (d) Water droplet on S3 membrane in the air, pushing down and moving up easily. (e) Oil contact angle on S3 membrane in the air. (f) Water droplet on S3 membrane surface in oil, pushing down and moving up. (g) Oil droplet on S3 membrane surface in water.

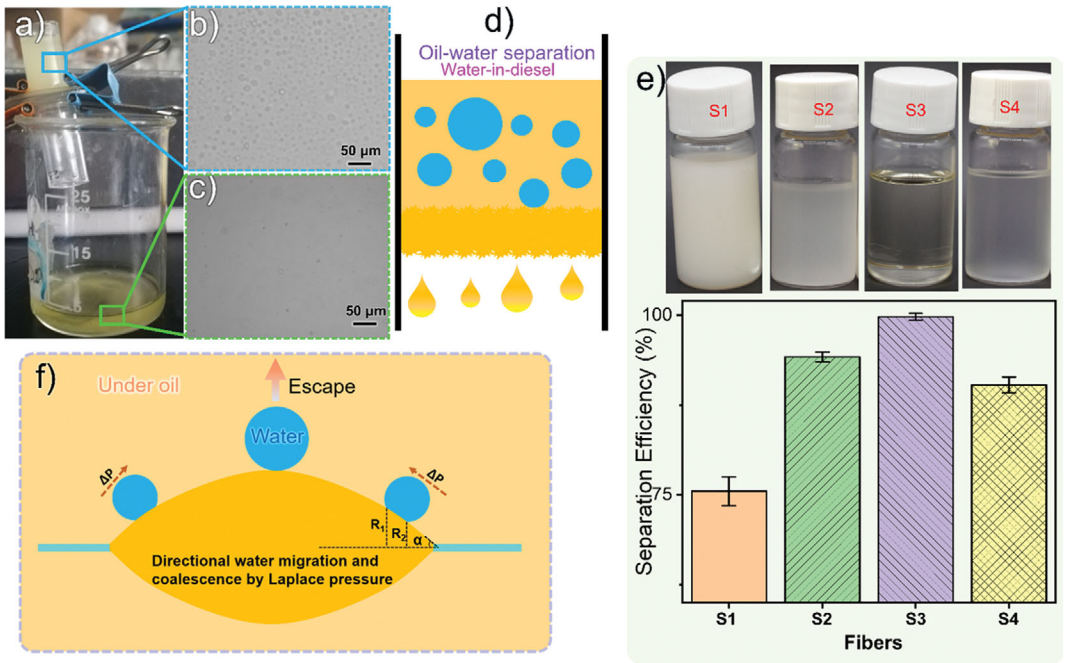

Fig. 6. (a) Image of oil-water emulsion separation device and diagram of the process. (b) and (c) Optical microscopy images of water-in-oil emulsion before (up) and after (down) separation. (d) Selective separation mechanisms of water-in-oil emulsions. (e) Emulsion separation efficiency on different surfaces and macro images. (f) Schematic diagram of directional water droplets migration and coalescence on the spindle-knots.

3. The Separation Mechanism of the Spindle-knotted Structured Membranes

It is traditionally thought to enhance the ability of hydrophobic surfaces to purity oil and form a stable oil layer on superoleophilic surface [27-29]. This layer keeps the membrane away from the water droplet. Therefore, the superoleophilic chemical properties of fibers play a significant role in improving the purity of oil performance. However, only hydrophobic chemical properties are difficult to obtain excellent oil purity performance. The experimental results also show that the spindle-knotted structure on the fibrous membranes is the key to improving the oil purity performance. In this section, the spindle-knotted structured membranes were used to visually how spindle structures on membrane do enhance the escaping of water droplets in the water-in-oil emulsions. The photograph

and optical microscopy images show the milky and opaque water-in-oil emulsion shown in Fig. 6(a) to Fig. 6(c), further confirming the high separation efficiency of the membrane. As illustrated in Fig. 6(d), due to the hydrophobicity and lipophilicity of the membrane, oil droplets will quickly penetrate through the membrane, and water droplets are blocked outside, thus achieving the purified oil. To reveal the separation performance of spindle-knotted structure membranes for water-in-oil emulsion, four membranes prepared for were used, and it can be seen that the emulsion separation efficiency of the above four membranes is 75.5, 94.2, 99.1, 90.3%, respectively, as shown in Fig. 6(e). As the separation efficiency increased, the transparency of the separated emulsion increased. The main driving force on a single spindle was the Laplace pressure difference (ΔP) [21,30,31] derived from curvature gradient at the two respective sides of the water droplet on the spindle, which can be represented as:

$$P_1=(\gamma_w-\gamma_o)\frac{1}{R_1} \tag{2}$$

$$P_2=(\gamma_w-\gamma_o)\frac{1}{R_2} \tag{3}$$

$$\Delta P=P_2-P_1=(\gamma_w-\gamma_o)\left(\frac{1}{R_2}-\frac{1}{R_1}\right)>0 \tag{4}$$

Here γ_w and γ_o are the surface tension of water and the oil, R_1 and R_2 are the local radii of the spindle on either side of the water droplet. The direction of the pressure difference was toward the center of spindle structure because R_1 was greater than R_2, so the ΔP from the gradient of the spindle shape. Where there was no pressure difference (ΔP) on the surface without spindle-knotted structures such as S1 fibrous membrane, thus, the fiber could not cause motion of water droplets in the oil.

Just as shown in Fig. 6(f), the difference in Laplace pressure stems from the gradient of spindle-knotted structure. The results indicate that these water droplets are able to be collected and escape from the spindle knots. It is well known that although the fiber surfaces are superoleophilic, the water residue problem is mainly caused by the deposition or adsorption of micro/nanoscale water droplets on the separation process. In contrast, the hydrophobic spindle-knotted structures allow water droplets to undergo directional motion under the action of Laplace pressure while the oil droplets can pass through the gap between the membranes. These properties can effectively decrease adsorption or deposition of tiny water droplets on the fiber and improve the purity of oil. The construction of superhydrophobic spindle knots is a new method of improving the purification of the oil. This analysis demonstrated that tiny water droplets could aggregate and form large ones; the reduced surface energy was then converted to kinetic energy and then the droplets escape from the spindle-knotted structure.

CONCLUSIONS

In summary, inspired by spider silk, we conceived a facile approach from modified coaxial electrospinning of PMMA/PS/SiO_2 membranes to fabricate superhydrophobic and superoleophilic spindle-knotted structured fibrous membranes for removing water droplets from water-in-oil emulsions. In this modified coaxial electrospinning, the inner needle is more prominent than the outer needle. By regulating the concentration of PS in the outer solution to the effect of corner flow, spindle-knotted structures were obtained with different morphologies. The emulsion separation experiments demonstrate that the spindle knotted structures have good water removal performance, high permeability and recyclability, and can be used for the separation of surfactant stability emulsions. Through this composite surface, tiny water droplets can be captured, aggregated, grown and even separated from the surface under the water-in-oil emulsion. Consequently, we believe that the spindle-knotted structure membranes we fabricated are a promising option for water-in-oil emulsion separation.

ACKNOWLEDGEMENTS

This work was financially supported by the National Key Research and Development Program of China (No. 2018YFA0702304) and Science and Development Key R&D Program of Changchun City (No. 21ZY28).

CONFLICT OF INTEREST

There are no conflicts to declare.

REFERENCES

1. J. Wang, F. Han, Y. Chen and H. Wang, *Sep. Purif. Technol.*, **209**, 119 (2019).
2. C. H. Peterson, S. D. Rice, J. W. Short, D. Esler, J. L. Bodkin, B. E. Ballachey and D. B. Irons, *Science*, **302**, 2082 (2003).
3. W. Zhang, N. Liu, Y. Cao, X. Lin, Y. Liu and L. Feng, *Adv. Mater. Interfaces*, **4**, 1700029 (2017).
4. B. Wang, W. Liang, Z. Guo and W. Liu, *Chem. Soc. Rev.*, **44**, 336 (2015).
5. E. S. Dmitrieva, T. S. Anokhina, E. G. Novitsky, V. V. Volkov, A. V. Volkov and I. L. Borisov, *Polymers*, **14**, 980 (2022).
6. L. Zhang, H. Li, X. Lai, X. Su, T. Liang and X. Zeng, *Chem. Eng. J.*, **316**, 736 (2017).
7. Q. Fan, T. Lu, Y. Deng, Y. Zhang, W. Ma, R. Xiong and C. Huang, *Sep. Purif. Technol.*, **297**, 121445 (2022).
8. A. Huang, L. H. Chen, C. C. Kan, T. Y. Hsu, S. E. Wu, K. K. Jana and K. L. Tung, *J. Membr. Sci.*, **566**, 249 (2018).
9. N. Chen and Q. Pan, *ACS Nano*, **7**, 6875 (2013).
10. J. Hu, J. Zhu, C. Jiang, T. Guo, Q. Song and L. Xie, *Colloids Surf. A Physicochem. Eng. Asp.*, **577**, 429 (2019).
11. L. Zhang, Y. Zhang, P. Chen, W. Du, X. Feng and B. F. Liu, *Langmuir*, **35**, 11123 (2019).
12. C. Li, L. Wu, C. Yu, Z. Dong and L. Jiang, *Angew. Chem. Int. Ed.*, **56**, 13623 (2017).
13. W. Ji, H. Wang, Y. Yao and R. Wang, *Cellulose*, **26**, 6879 (2019).
14. M. Ge, C. Cao, J. Huang, X. Zhang, Y. Tang, X. Zhou, K. Zhang, Z. Chen and Y. Lai, *Nanoscale Horiz.*, **3**, 235 (2018).
15. W. Zhou, S. Li, Y. Liu, Z. Xu, S. Wei, G. Wang, J. Lian and Q. Jiang, *ACS Appl. Mater. Interfaces*, **10**, 9841 (2018).
16. N. Naseeb, A. A. Mohammed, T. Laoui and Z. Khan, *Materials*, **12**,

212 (2019).
17. W. Fang, L. Liu and G. Guo, *Chem. Eur. J.*, **23**, 11253 (2017).
18. R. Pan, M. Cai, W. Liu, X. Luo, C. Chen, H. Zhang and M. Zhong, *J. Mater. Chem. A.*, **7**, 18050 (2019).
19. A. Azimi and P. He, *MRS Commun.*, **10**, 129 (2020).
20. J. Li, W. Jiao, Y. Wang, Y. Yin and X. He, *Chem. Eng. J.*, **434**, 134710 (2022).
21. Z. Zhang, N. Han, L. Tan, Y. Qian, H. Zhang, M. Wang, W. Li, Z. Cui and X. Zhang, *Langmuir*, **35**, 16545 (2019).
22. J. Zhang, X. Huang, Y. Xiong, W. Zheng, W. Liu, M. He, L. Li, J. Liu, L. Lu and K. Peng, *Sep. Purif. Technol.*, **280**, 119824 (2022).
23. W. Yu, Q. Ma, X. Li, X. Dong, J. Wang and G. Liu, *Mater. Lett.*, **120**, 126 (2014).
24. C. Chen, L. Chen, D. Weng, S. Chen, J. Liu and J. Wang, *Sep. Purif. Technol.*, **288**, 120621 (2022).
25. J. Li, X. Zhou, J. Li, L. Che, J. Yao, G. McHale, M. K. Chaudhury and Z. Wang, *Sci. Adv.*, **3**, 19 (2017).
26. L. Yong-Qiang, C. Wen-Hui and L. Ling, *Microgravity Sci. Technol.*, **29**, 65 (2017).
27. H. Li, G. Zhu, Y. Shen, Z. Han, J. Zhang and J. Li, *J. Colloid Interface Sci.*, **557**, 84 (2019).
28. J. Wu, H. Li, X. Lai, Z. Chen and X. Zeng, *Ind. Eng. Chem. Res.*, **58**, 8791 (2019).
29. E. Mosayebi, T. Zhao, S. Azizian and D. Zhao, *Surf. Interfaces*, **27**, 101464 (2021).
30. K. Li, J. Ju, Z. Xue, J. Ma, L. Feng, S. Gao and L. Jiang, *Nat. Commun.*, **4**, 2276 (2013).
31. J. Zhang, L. Liu, Y. Si, S. Zhang, J. Yu and B. Ding, *Nanotechnology*, **32**, 495704 (2021).